TUTORIAL | MAY 13 2024

Special Collection: Special Topic Collection: Tutorials in Sum-Frequency Generation Spectroscopy 2024

Joshua M. Taylor 💿 ; John C. Conboy 🔀 💿



Biointerphases 19, 031201 (2024) https://doi.org/10.1116/6.0003594





Articles You May Be Interested In

Creation and Relaxation of Phospholipid Compositional Asymmetry in Lipid Bilayers Examined by Sum-Frequency Vibrational Spectroscopy

AIP Conference Proceedings (August 2010)

Issues with lipid probes in flip-flop measurements: A comparative study using sum-frequency vibrational spectroscopy and second-harmonic generation

J. Chem. Phys. (August 2024)





Cite as: Biointerphases 19, 031201 (2024); doi: 10.1116/6.0003594 Submitted: 4 March 2024 · Accepted: 23 April 2024 ·

Published Online: 13 May 2024







Joshua M. Taylor 匝 and John C. Conboy^{a)} 🔟

AFFILIATIONS

Department of Chemistry, University of Utah, 315 South 1400 East RM. 2020, Salt Lake City, Utah 84112

Note: This paper is part of the Biointerphases Special Topic Collection Tutorials in Sum-Frequency Generation Spectroscopy 2024. a) Author to whom correspondence should be addressed: John.Conboy@utah.edu

ABSTRACT

Planar supported lipid bilayers (PSLBs) are an ideal model for the study of lipid membrane structures and dynamic

vibrational spectroscopy (SFVS). In this paper, we describe the construction of asymmetric PSLBs and the basic SFVS theory needed to understand and make measurements on these membranes. Several examples are presented, including the determination of phospholipid orientation and measuring phospholipid transmembrane translocation (flip-flop).

I. INTRODUCTION

Scientists have been captivated by cells for hundreds of years, intrigued by their functions and interactions with the external environment. Robert Hooke, an English polymath, was the first to examine cells in the 1660s when looking at fine structures of cork through a primitive microscope.^{1,2} It was Hooke who coined the term cell from the Latin "cellula" in reference to a room or chamber, which was used to describe the dividing cell walls seen in the cork microstructures he examined. Soon after Hooke's initial findings, Dutch scientist Antonie van Leeuwenhoek was one of the first to observe the microbial world with a custom-made microscope.^{3,4} He would emerge as the pioneer of microbiology, founding a field essential for comprehending not just the microscopic world around us, but also the cells that form us. Since these initial discoveries, our knowledge of cells has grown at an astonishing rate, but uncertainties on specific aspects still exist, keeping the field active. One of the more fascinating aspects of the cell is the component that separates the inner workings of the cell from the outside world, a component that the cell has its very etymology in the plasma membrane (PM). The history and scientific progression of our understanding of the PM has taken over 200 years of research after Hooke's and van Leeuwenhoek's initial discoveries with contributions from prominent scientists such as John William

Strutt, Charles Ernest Overton, and Irving Langmuir among others. 5,6 The most widely accepted description of the PM was proposed in 1972 by Seymour Singer and Garth Nicolson. Their fluid mosaic model characterized the PM as a dynamic system consisting of a phospholipid bilayer containing an outer (exoplasmic) and inner (cytoplasmic) leaflet that are adorned with proteins, glycoproteins, cholesterol, and other molecules that aide in the stability and functionality of the PM. 7,8 As our knowledge of the PM developed, it was discovered that different phospholipid types are asymmetrically distributed between the two leaflets of the bilayer, with the lipid composition between the two leaflets being unequal and nonrandom. 9-11 A primary example of this lipid asymmetry is the observation of phospholipids containing the serine (PS) head group, being found almost exclusively in the cytosolic leaflet of the PM in eukaryotic cells. 11,12 This lipid asymmetry is required for a host of cellular signaling pathways, but the origin of the cell's ability to create and maintain this lipid asymmetry is still under debate. Related to lipid asymmetry is another interesting phenomenon called "phospholipid transmembrane translocation" or more affectionately referred to as "lipid flip-flop." Lipid flip-flop is the traversing of a phospholipid from one leaflet of the membrane to the other leaflet [Fig. 1]. 15,17 Phospholipid flip-flop has long been thought to be a protein-mediated process where phospholipid-specific, ATP-driven "flippases" and "floppases" mediate the movement of

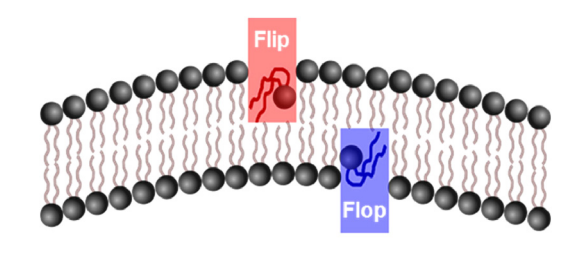


FIG. 1. Visual representation of a phospholipid flip-flop.

these lipids to maintain the lipid asymmetry observed within the membrane.¹⁷⁻²⁰ However, work on model systems that lack these enzymes shows that enzyme-free or native flip-flop does occur, although the measured rate varies from study to study, with rates so slow that they are of little biological importance, while other experiments suggest the exact opposite.²¹,

The discrepancies seen in the results of flip-flop experiments are in part due to the complexities of measuring the process. The measurement of lipid asymmetry and lipid flip-flop in membranes is a nontrivial undertaking, as there is a lack of analytical techniques that are sensitive or specific enough to measure flip-flop without compromising the membrane and possibly introducing error within the measurement with the introduction of foreign labeled molecules or reagents. The primary analytical techniques and models used to measure lipid flip-flop can generally be broken down into two categories, labeled or label-free techniques. Labeled methods employ the use of a modified lipid containing a chemical tag or label that can be altered to measure lipid flip-flop kinetics. Examples of labeled methods include electron spin resonance (ESR) that utilize a lipid containing a stable radical label such as 2,2,6,6-tetramethyl-1-piperidinyloxy (TEMPO).²³ In addition, fluorescence can be used where the lipid is modified with a fluorescent probe such as nitrobenzoxadiazole (NBD) or pyrene.²⁴ Arguments have been made on the validity of these labeled lipids, as one would expect the addition of a large, bulky label to inherently alter the kinetics of lipid translocation due to the alteration of the chemical nature of the lipid. The other set of analytical techniques used to measure lipid flip-flop have been deemed "label-free" and include sophisticated techniques such as small angle neutron scattering (SANS),^{29,30} nuclear magnetic resonance (NMR),³¹ and sum-frequency vibrational spectroscopy (SFVS).³² These techniques use deuterated analogs of native lipids to circumvent the use of bulky chemical labels. These deuterated analogs are a preferable alternative to labeled lipids, as they do not drastically change the chemical nature of the lipid but allow one to differentiate lipids in the membrane.

In addition to the set of analytical methods that can be used to measure lipid flip-flip and asymmetry, historically, two lipid membrane models have been employed in these flip-flop studies, vesicle systems, and planar supported lipid bilayers (PSLBs). These model membranes have long been used to examine how individual lipid components influence the physical, mechanical, and biological properties of membranes. 23,33,34 Not all these models are created equal, however, and there is constant debate on which models best capture the "true" behavior of in vivo phospholipid bilayers. Both models are commonly used and have their advantages and disadvantages in studying lipid flip-flop kinetics. Vesicles are said to capture the tension-free nature of a cell, but vesicle creation limits the control of other characteristics such as packing and control over the asymmetric distribution of deuterated and proteated lipids between the leaflets of the membrane. In SANS, the creation of fully proteated and fully deuterated vesicles and modeling the rate of intervesicle exchange in conjunction with flip-flop is used to resolve this issue,³⁰ while in NMR, the use of methyl-β-cyclodextrin (MβCD) is used to create asymmetric vesicles.³¹ PSLBs benefit from having tight control of lipid packing and distribution of lipids within the leaflets when using the Langmuir-Blodgett/Langmuir-Schaefer (LB/LS) method but do not have a curvature and have a defined edge to the bilayer. In addition, the influence that the solid support exerts on the bilayer in PSLBs has brought up questions regarding the efficacy of using such models. However, experiments have shown that PSLBs show the same membrane fluidity in both leaflets, within error, of vesicle systems, making them comparable.

Our group has demonstrated that lipid asymmetry, lipid flipflop, membrane structure, and other important physical characteristics of a bilayer can be measured directly on PSLBs using SFVS. 21,32,37-50 Examples of measurements that have been made on membranes using SFVS include the measurement of alkyl chain tilt angles using different sum-frequency polarization states⁴⁴ as well as determining important kinetics such as the rate of flip-flop of native phospholipids and the influence that cholesterol and integral membrane peptides have on the rate of flip-flop. 37,51-53 Tutorial is designed to review the basic SFVS theory as applied to measuring lipid membrane structures and dynamics, and it is hoped that it will stimulate creativity and spark inspiration in those who wish to conduct experiments on membranes or similar systems & using SFVS. Additional information on the construction of PSLBs, N how asymmetric PSLBs generate sum-frequency, the interpretation $\frac{2}{12}$ and treatment of data, a brief description of the SFVS instrumentation, and a review of select experiments is also presented.

II. EXPERIMENT

The experiment section is designed to first describe the creation of PSLBs. Next, a brief review of the sum-frequency theory required to understand and measure phospholipid structures, as well as phospholipid flip-flop in PSLBs, is discussed. Lastly, a brief description of the instrumentation and equipment is given for those interested in conducting these types of SFVS experiments.

A. Langmuir-Blodgett/Langmuir-Schaefer method

The Langmuir-Blodgett/Langmuir-Schaefer (LB/LS) method has its beginnings nearly 100 years ago when interest in studying the surface characteristics of simple films of oils on aqueous surfaces and deposition of said films became readily measurable with the invention of the Langmuir trough. 54,55 Only the salient points on the construction of PSLBs using the LB/LS method will be discussed. A wonderfully detailed review by Olivera et al. on the history and present state of these techniques is available and reading is encouraged for those interested in the historical and scientific background of these techniques.

Before a discussion on the generation of PSLBs, it is important to discuss the solid support that is used to create them. The choice of substrate, or solid support, is important in the successful creation of a bilayer and in the measurements of SFVS of these assemblies. The substrates used in our experiments have typically been custom trapezoidal IR-grade fused silica prisms (Almaz Optics, Marlton, NJ), which can be seen in Fig. 2. Optical-grade fused silica is used for multiple reasons, with the primary reasons being its general chemical stability in water and buffers, its transmission of the aliphatic IR region (2700-3100 cm⁻¹), its relatively high refractive index (~1.45), and the hydrophilicity of the surface. The trapezoidal shape of our prisms allows for an appropriate angle to let the visible and IR beams enter normally through the faces of the prism for the total internal reflection (TIR) of the incident and generated sum-frequency at the silica/water interface. The use and importance of TIR for SFVS measurements will be discussed in Sec. II B. Another important aspect is the optical smoothness and the cleanliness of the surface, as an uneven surface with organic debris or other contaminants can hinder successful bilayer formation and has the potential to generate unwanted SFVS at the surface. Our group has adopted the following cleaning procedure for our prisms: Prisms are placed in an UV-ozone cleaner (Jetlight Co., Irvine, CA) for 10 min and subsequently immersed in a piranha solution prepared with three parts 18 M sulfuric acid to one part 30% H₂O₂ for a minimum of 60 min. (Caution: This is a highly corrosive solution and a strong oxidant that reacts violently with organic solvents. Extreme caution must be taken when handling the piranha solution.) Afterward, prisms are rinsed with copious amounts of nanopure water with a minimum resistivity of 18.2 M Ω , dried under a light stream of nitrogen, treated with argon plasma (Harrick Scientific, Ithaca, NY) for 5 min and submerged in the trough subphase soon after to avoid any dust or other contaminants that may deposit onto the surface from the air. Naturally, the type of prisms used and the cleaning procedures will change on a laboratory to laboratory basis and one should always determine what procedure is adequate for the work being done in their laboratory, but the quality and cleanliness of the planar support should never be overlooked when working with PSLBs.

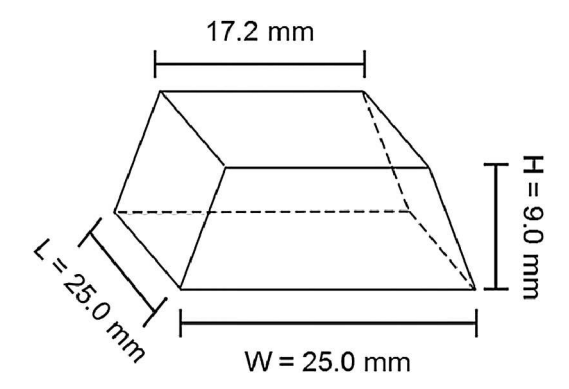


FIG. 2. Schematic of the fused silica prisms used as a PSLB substrate. The trapezoidal design is used to allow for near normal incidence of the incoming beams on the slanted surfaces and also to allow for total internal reflection of the incident and reflected beams at the prism base.

PSLB generation using the LB/LS method is widely discussed in the literature, and a concise overview follows. ^{32,34,57-60} PSLBs start with the construction of a phospholipid monolayer on a prism substrate surface via a Langmuir–Blodgett transfer, which can be seen in Fig. 3(a). The prism is fully submerged within the subphase

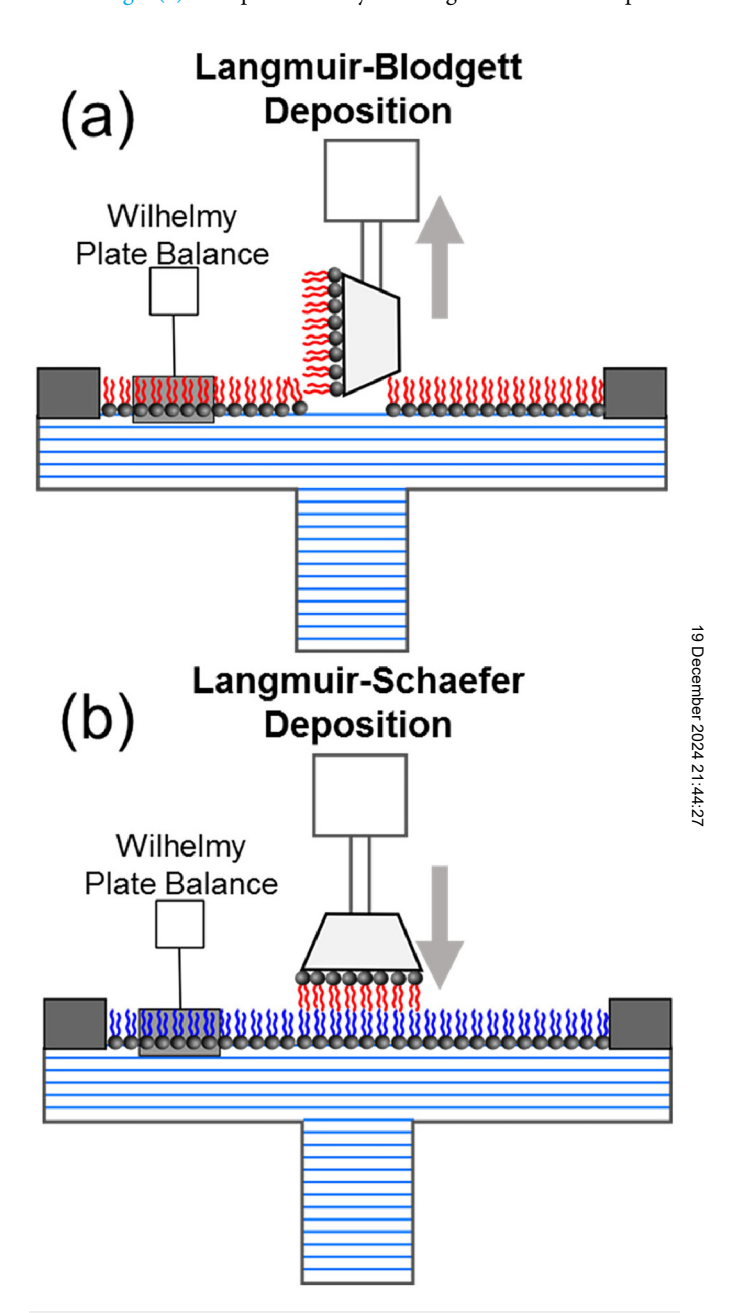


FIG. 3. Visual description of the LB/LS method used to generate a PSLB. (a) A monolayer of a deuterated lipid (red) is first deposited using the Langmuir–Blodgett deposition method. (b) A second monolayer composed of the proteated form of the lipid (blue) is made and the PSLB is generated through a Langmuir–Schaefer deposition.

of a Langmuir trough (KSV, Helsinki, Finland), and a platinum Wilhelmy plate is used to measure the lateral surface pressure of the lipids on the surface of the subphase. In lieu of a platinum plate, paper plates can also be used with similar success. Before the addition of lipid on the subphase surface, the lateral surface pressure is zeroed and the barriers are compressed. If no contaminants are present on the subphase surface, the lateral surface pressure should remain relatively unchanged upon compression. Lipid solutions in chloroform (typically 1 mg of lipid per 1 ml of CHCl₃) are then deposited at the air-water interface of the trough and allowed to equilibrate for 10 min to allow for solvent evaporation. The trough barriers are then brought in at a rate of 3 mm/min to bring the lateral surface pressure of the lipids to 30 mN/m, the approximate lateral surface pressure of vesicle systems (30-35 mN/m).61 The prism is then brought up through the subphase at a rate of 3 mm/min to deposit the Langmuir-Blodgett layer to the substrate. This monolayer is stable in air for some time and can remain in air as preparations for the next step take place. The trough is then cleaned by removing the current subphase with an aspirator, the surface of the trough is wiped down with a small amount of isopropyl alcohol, and the trough is rinsed thoroughly with copious amounts of nanopure water. The prism is then flipped horizontally and a second monolayer is created on the trough similar to the first monolayer. The prism is then submerged through the subphase to complete the Langmuir-Schaefer (LS) transfer, which is illustrated in Fig. 3(b). The Schaefer transfer requires that the prism be directly parallel to the subphase surface for the LS transfer to be successful. Slight angles in the substrate during the LS transfer can cause a poorly formed bilayer or the complete failure of bilayer formation. The prism + PSLB is then placed in a custom cell holder where the surface containing the bilayer can remain in an aqueous environment. The subphase in the cell holder is then replaced with D₂O through ports to remove SFVS spectral interferences caused by water. It should be noted that it is very crucial that PSLBs remain in an aqueous environment as the integrity and stability of the membrane is greatly diminished in air. It should also be noted that once a bilayer is formed, flip-flop begins to occur and SFVS measurements should be conducted soon after bilayer formation to avoid potential loss of compositional asymmetry. That being said, the type of lipid being studied will dictate the rate of flip-flop; some bilayers maintain asymmetry at room temperature, while others flip-flop rapidly. For those lipids that move rapidly at room temperature, it is suggested that a temperature bath or cold room be used for the trough to avoid rapid flip-flop of the PSLB. The LB/LS method is a powerful tool that allows for control over the lateral surface pressure of the membrane, as well as independent control over the composition of the two leaflets of the PSLB, such as the creation of an isotopically asymmetric distribution of lipids between the leaflets for the measurement of SFVS, which will be discussed in greater detail below.

B. SFVS theory and application

Section II B is designed to give a basic introduction on the theory of SFVS, the spectroscopy of lipids in PSLBs, as well as the types of measurements that can be made on PSLBs, such as phospholipid orientation and flip-flop. Nonlinear optics (NLO) is a

fascinating yet difficult subject, requiring a deep understanding of optics and mathematics to truly appreciate the field. To make these experiments more accessible to those with a limited knowledge of NLO, no attempt will be made to give an in-depth, detailed description of the underlying optical physics, and all theory will be described through an application-based lens. More detailed descriptions on sum-frequency and NLOs, 62-64 as well as more digestible reviews from these tutorial series, 65-67 are available for a more complete description of sum-frequency.

1. SFVS on PSLBs

Sum-frequency is a coherent, nonlinear, two-photon event in which a visible (ω_{Vis}) and IR (ω_{IR}) laser source are both spatially and temporally overlapped at an interface and a resulting third photon is generated at the sum of the two incident frequencies (ω_{SFG}) ,

$$\omega_{\rm SFG} = \omega_{\rm Vis} + \omega_{\rm IR}. \tag{1}$$

The symmetry constraints on SFVS limits the generation of ω_{SFG} to material that have a lack of inversion symmetry or at interfaces where inversion symmetry of the bulk phase is broken. ⁶² This characteristic of SFVS makes it a wonderful spectroscopic method to study interfaces or surfaces. The signal intensity, or the likelihood of sum-frequency photons being generated from the two incoming photons, can be described by way of the following equation:

$$I_{SFG} = \left| \tilde{f}_{SF} f_{Vis} f_{IR} \chi^{(2)} \right|^2, \tag{2}$$

where $\chi^{(2)}$ (pronounced chi two) is the second-order nonlinear susceptibility tensor, a 27-element third-rank tensor that describes the surface response to the applied electric fields of the incident photons and the generated sum-frequency photon. 62 The symmetry of the interface dictates which $\chi^{(2)}$ elements are nonzero. For interfaces between two isotropic media, such as our PSLBs at the silica-water interface, the surface possesses $C_{\infty v}$ symmetry and the 27-element tensor is reduced to three nonvanishing elements, χ_{zzz} , $\chi_{zyy} = \chi_{zxx}$, and $\chi_{yzy} = \chi_{xzx} = \chi_{yyz} = \chi_{xxz}$, simplifying $\chi^{(2)}$ considerably. The $\chi^{(2)}$ elements are selected through proper selection of the polarization states of the incident and emitted photons. The subscripts of $\chi^{(2)}$ denote the orientation of the electric fields of the sum-frequency, visible, and IR photons relative to a coordinate system at the surface. The term f_{SF} in Eq. (2) is the nonlinear geometric Fresnel coefficient of the generated sum-frequency, and f_{Vis} and f_{IR} are the geometric Fresnel coefficients for the visible and IR fields, respectively. The optical Fresnel coefficients are used to describe how light behaves when it hits the boundary between two different materials, such as the interface between silica and water. The Fresnel coefficients tell us how much of the light (electric field magnitude) is reflected and transmitted from the interface. The coefficients are calculated based on the angle at which the light hits the interface, the indices of refraction of the materials and the polarization of the light [whether the light waves are polarized parallel (p-polarized) or perpendicular (s-polarized) to the plane of incidence]. A more in-depth discussion on the Fresnel coefficients and their importance in interpreting SFVS data is available. 62,64,68 The $\chi^{(2)}$ tensor contains a resonant $(\chi_R^{(2)})$ and

nonresonant $(\chi_{NR}^{(2)})$ component,

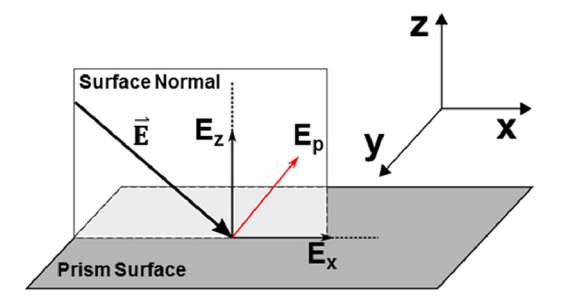
$$\chi^{(2)} = \chi_{R}^{(2)} + \chi_{NR}^{(2)}.$$
 (3)

The nonresonant contribution to the sum-frequency signal intensity is typically very small for dielectric materials, such as our fused silica substrate, and can often be ignored. The resonant contribution for sum-frequency is defined as

$$\chi_{\rm R}^{(2)} = N \sum_{x=1}^{m} \frac{\langle A_k M_{ij} \rangle_x}{\omega_{\rm v} - \omega_{\rm IR} - i\Gamma_{\rm v}},\tag{4}$$

where N is the number of sum-frequency active molecules at the surface, m is the number of vibrational transitions, A_k and M_{ij} are the IR and Raman transition probabilities, respectively, ω_{v} describes the frequency of a known vibrational mode at the surface, ω_{IR} is the frequency of the input IR laser beam, and Γ_{ν} is the intrinsic linewidth of the vibrational mode transition. The summation and bra and ket notation in Eq. (4) indicate the summation over the ensemble orientation average for these transitions. Equation (4) can be examined in individual parts to better understand how to optimize $\chi_R^{(2)}$ and by extension optimize the SFVS signal intensity in Eq. (2). First, the value N outside of the summation tells us that the more sum-frequency active modes are located at the surface, the larger $\chi^{(2)}$ becomes, which, in turn, increases the SFVS signal intensity. It is also critical to note that there is a squared dependence to N, which can be seen in Eq. (2), where the signal intensity is proportional to $\chi^{(2)}$ squared. Second, the numerator of Eq. (4) shows that for $\chi^{(2)}$ to be nonzero, the transition being probed at the surface must be both IR- and Raman active. That is, if the transition probability is zero for one or both, $\chi^{(2)}$ will equal zero and no sum-frequency will be generated. Third, the denominator of Eq. (4) tells us that the closer the frequency of the IR laser beam is to a vibrational mode at the surface (i.e., as ω_{IR} approaches ω_{v}), the denominator approaches zero and $\chi^{(2)}$ increases as a result. Lastly, it is important to note that $\chi^{(2)}$ is a complex quantity that contains both a real and an imaginary component. The measured SFVS intensity is the absolute value squared [Eq. (2)], and as a result, information regarding the imaginary or phase information of the measured sum-frequency is lost. While crucial in truly understanding the nature of $\chi^{(2)}$, this phase information is beyond the scope of the discussions within this tutorial, and additional reading is encouraged for those interested in the extraction of the complex components.⁶⁹ If the IR frequency is tunable, we can access different vibrational modes that are active on the surface, which allows for the collection of SFVS spectra. Another important aspect of $\chi^{(2)}$, and SFVS as a whole, is the polarization of the incoming electric fields. As previously mentioned, the polarization of the incident fields will dictate which of the remaining $\chi^{(2)}$ components can be accessed. In SFVS, p-polarized and s-polarized IR fields are used to probe vibrational transitions parallel and perpendicular to the surface normal, respectively [Fig. 4]. For example, when using ssp polarization (by convention, the order of polarization is from the highest-energy to the lowest-energy photon, i.e., sum-frequency, visible, and then IR), any vibrational modes parallel to the surface normal will be SFVS active [Fig. 4(a)], while if the polarization is

(a) p-polarization



(b) s-polarization

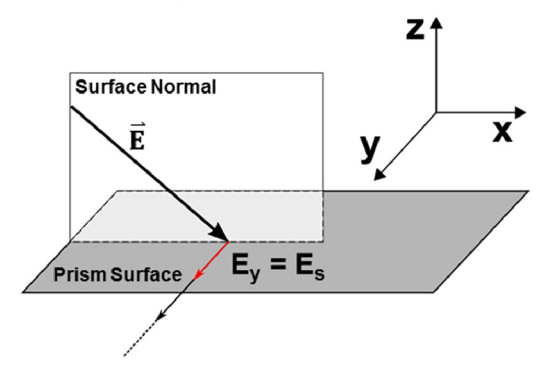


FIG. 4. Representation of (a) p-polarized and (b) s-polarized light. A p-polarized IR source has an electric field component parallel to the surface normal and is capable of accessing vibrational modes that have a dipole moment component parallel to the surface normal, while an s-polarized IR source has an electric field perpendicular to the surface normal and is capable of accessing vibrational modes perpendicular to the surface normal.

sps, the vibrational modes perpendicular to the surface normal will be observed [Fig. 4(b)].⁴⁴ By collecting SFVS spectra in both ssp and sps polarizations, information regarding the orientation of the lipid acyl chains and headgroup is readily retrieved. The specifics of this approach are discussed below.

Another factor that exists to optimize the SFVS signal intensity is the geometry of the experiment. A strong enhancement of SFVS will occur under total internal reflection (TIR), ⁶⁸ which occurs when the incident angles of the visible and IR sources are greater than the critical angle θ_C ,

$$\theta_C = \sin^{-1}\left(\frac{n_2}{n_1}\right),\tag{5}$$

where n_1 and n_2 are the refractive index of the silica prism and the aqueous phase (D₂O), respectively. The critical angle of the IR at 2875 cm⁻¹ at the silica $(n = 1.407)^{70}$ D₂O $(n = 1.248)^{71}$ interface is 62.5° and the critical angle for the visible (532 nm) at the silica $(n = 1.461)^{70}$ D₂O $(n = 1.330)^{72}$ interface is 65.6°. To accommodate

the TIR of both IR and visible sources, the beams are typically combined at the interface with incident angles 63° and 69° to ensure that both beams are under TIR. Figure 5 shows the incident IR and 532 nm beams aligned to the prism. The prism is rotated to give angles of incidence of 63° and 69° for the IR and 532 nm beams, respectively [Fig. 5], to the surface normal of the square surface of the prism. The 67° cut of the prism is such that IR and green beams are near normal to the entrance face. The angle of the generated sum-frequency can be found using the following equation:

$$n_{\rm SFG}\omega_{\rm SFG}\sin(\theta_{\rm SFG}) = n_{\rm Vis}\omega_{\rm Vis}\sin(\theta_{\rm Vis}) \pm n_{\rm IR}\omega_{\rm IR}\sin(\theta_{\rm IR}).$$
 (6)

Here, n_{SFG} , n_{Vis} , and n_{IR} are the refractive index of the sumfrequency, visible, and IR photon, respectively, through the media, ω_{SFG} , ω_{Vis} , and ω_{IR} are the frequencies of the sum-frequency, visible, and IR photons, respectively, and θ_{SFG} , θ_{Vis} , and θ_{IR} are the angles of reflection from the surface normal for the sum-frequency, visible, and IR. Whether the IR component in Eq. (6) is added or subtracted is dependent on whether the visible and IR sources are copropagated or counter-propagated, respectively. The sum-frequency generated from a 532 nm visible and a 2875 cm⁻¹ IR source will be 461 nm and has a critical angle of 65.4° at the silica/ D₂O interface. The generated sum-frequency photon is emitted at an angle of 63.9° using Eq. (6), which under TIR, further enhances the SFVS response. The enhancement of sum-frequency under TIR is related to an increase in the nonlinear Fresnel coefficient found in Eq. (2), and the intricacies of this enhancement are described in detail in Dick et al.68 The emitted sum-frequency photon is closer in proximity to the visible source, as the visible source carries a major amount of the momentum of the generated sum-frequency photon.

By utilizing SFVS's polarization dependence and the PSLBs' distinct structure, one can easily determine the orientation of different functional groups within the bilayer. The alkyl chains in PSLBs are relatively well-ordered and oriented along the surface normal, with the chains in each leaflet oppositely oriented from each other. However, the symmetry constraints of SFVS make it highly sensitive to asymmetry at the surface, and if there is symmetry, sum-frequency cannot occur. For example, if there are

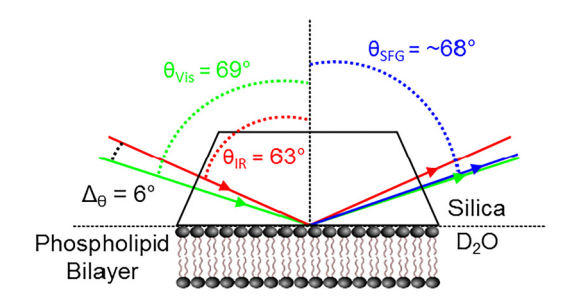


FIG. 5. Illustration of the incident IR and 532 nm beam alignment. The prism is rotated to give an IR and 532 nm incident angles of 69° and 63°, respectively. At these incidence angles, both the IR and the 532 nm incident beams are under TIR at the silica/D $_2$ O interface. The generated sum-frequency that is emitted at an angle of \sim 68° is also shown.

transition dipole moments that are oppositely oriented from one another at the surface, such as the opposite orientation of the alkyl chains in the opposing leaflets in a PSLB, the modes will be out of phase with each other, and a destructive interference of these phases results in no observable SFVS, which is illustrated in Fig. 6. However, if one were to intentionally prepare a PSLB in such a way where the opposing dipoles do not cancel, SFVS is possible. This is done by creating one leaflet with an unmodified, proteated lipid and also a second leaflet using an isotopically deuterated analog of that lipid. The two phospholipids within the leaflets will be chemically identical but have vibrational modes that are at different frequencies due to the isotropic substitution of H for D, creating asymmetry. As we scan the aliphatic region of the IR (2750–3050 cm⁻¹) for asymmetric PSLBs, we will see increases in SFVS as we approach a vibrational mode on the alkyl chain of our

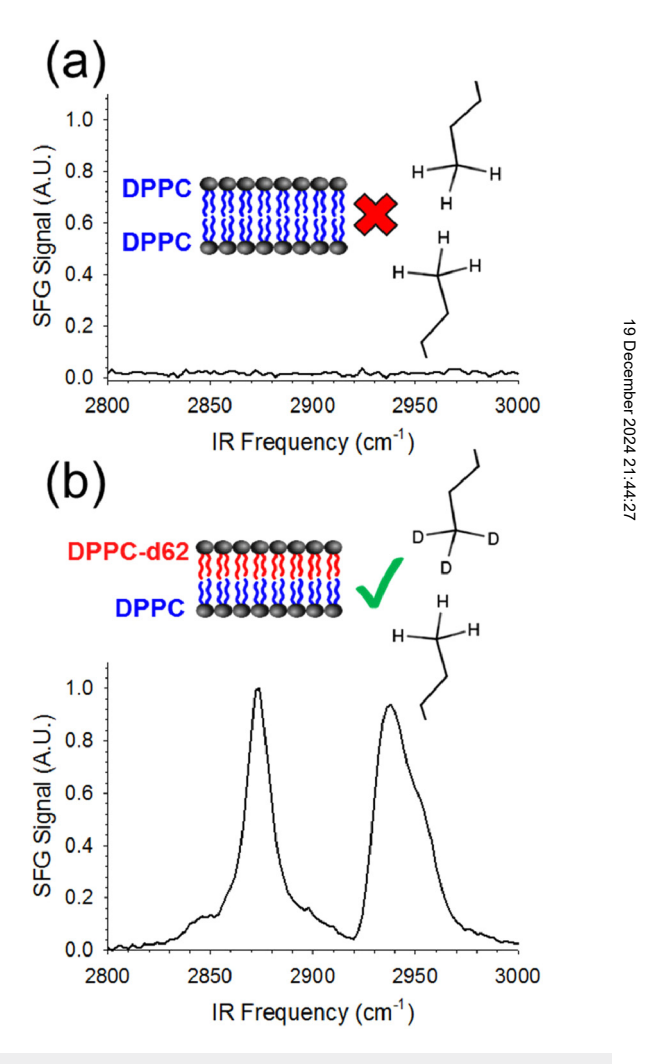


FIG. 6. Illustration of the asymmetry requirement to observe SFVS from a PSLB. (a) An SFVS spectrum of a symmetric DPPC bilayer and (b) an SFVS spectrum of an asymmetric DPPC/DPPC-d62 bilayer.

proteated lipids. When using *ssp* polarization (which, again, probes molecular vibrations parallel to the surface normal), the peaks that are generated in our SFVS spectrum can be seen in Fig. 6. These spectral features will be discussed in Sec. IV A.

2. SFVS orientation measurements

An important characteristic that can be measured using SFVS is the orientation of the alkyl chains and headgroups of the phospholipids of the PSLB. This is accomplished by changing the polarization of our incident beams to probe the dipole moments of the vibrational modes in different orientations of the PSLB. The SFVS spectra for ssp and sps polarizations can be used to determine the tilt angles by comparing the relative amplitudes of the SFVS signal for the methyl symmetric stretch (CH₃ v_s) mode of the terminal methyl group on the alkyl chains of the phospholipids at 2 876 cm $^{-1}$ and the CH₃ v_s mode of the choline headgroup at 2975 cm $^{-1}$. The *ssp* polarization state probes SFVS parallel to the surface normal of the membrane, while the sps polarization state probes SFVS vibrational modes with their transition dipole moments oriented perpendicular to the surface normal. Using the sumfrequency intensity of the CH₃ v_s and N-CH₃ v_s for both the ssp and the sps polarization states, the tilt angle (θ) of these functional groups is determined from the following expression assuming a delta function distribution:7

$$\theta = \operatorname{arccot}\left[\left(\frac{\chi_{\operatorname{ssp}}^{(2)}}{\chi_{\operatorname{sps}}^{(2)}} - \frac{1+R}{1-R}\right) \frac{1-R}{2R}\right]^{\frac{1}{2}},\tag{7}$$

where $\chi^{(2)}_{ssp}$ and $\chi^{(2)}_{sps}$ are the contributing, nonzero $\chi^{(2)}$ elements in the *ssp* and *sps* polarization configurations, and R is defined as

$$R = \frac{Q-1}{Q+2} \text{ or } \frac{Q+1}{Q-2} \text{ , where } Q = \left[\frac{3}{5} \left(\frac{1}{\rho} - \frac{4}{3} \right) \right]^{\frac{1}{2}},$$
 (8)

where ρ is the Raman depolarization ratio, an experimentally determined value that is 0.023 for the CH₃ v_s mode and 0.036 for the N-CH₃ v_s mode. Which form of R to use in Eq. (7) is dependent on the $\chi_{\rm ssp}^{(2)}$ to $\chi_{\rm sps}^{(2)}$ ratio, where if the ratio is positive, then the value for R that is less than 1 must be selected, whereas if the ratio is negative, the R value that is greater than 1 must be selected. For gel state lipids below the phase transition temperature, the gauche content within the alkyl chains is minimal and a near all-trans conformation is observed. At 4,75–79 The well-ordered chain structure of gel phase lipids allows for the assumption of a delta function to be used for the orientation distribution of the terminal methyl groups. Caution should be observed, however, as the delta function is not valid in PSLBs where disorder, normally in the form of gauche defects in the alkyl chains, is present. The $\chi_{\rm ssp}^{(2)}$ to $\chi_{\rm sps}^{(2)}$ ratio can be determined by finding the individual values for $\chi_{\rm ssp}^{(2)}$ and $\chi_{\rm sps}^{(2)}$ using the following equations:

$$\chi_{\rm ssp}^{(2)} = \left(\frac{A_{\rm ssp}}{\left|\tilde{f}_y^{\rm SF} f_y^{\rm vis} f_z^{\rm IR}\right|^2}\right)^{\frac{1}{2}},\tag{9}$$

$$\chi_{\text{sps}}^{(2)} = \left(\frac{A_{\text{sps}}}{\left|\tilde{f}_{y}^{\text{SF}}f_{z}^{\text{vis}}f_{y}^{\text{IR}}\right|^{2}}\right)^{\frac{1}{2}},\tag{10}$$

where $A_{\rm ssp}$ and $A_{\rm sps}$ are the amplitudes of the mode determined by a fit of the SFVS spectra and $\tilde{f}^{\rm SF}$, $f^{\rm vis}$, and $f^{\rm IR}$ are the geometric Fresnel coefficients for the particular optical configuration used. ^{62,63}

3. SFVS measurement of lipid flip-flop

In addition to spectroscopic and structural information, SFVS is also capable of directly measuring kinetic processes such as phospholipid flip-flop. The example in Fig. 7 shows a bilayer composed of a 1,2-dipalmitoyl-sn-glycero-3-phosphocholine (DPPC) monolayer in one leaflet and its deuterated analog, DPPC-d62, in the opposing leaflet. When this asymmetric PSLB is first generated, there is a complete asymmetric distribution of the proteated and deuterated lipids in each leaflet, giving rise to a maximum intensity

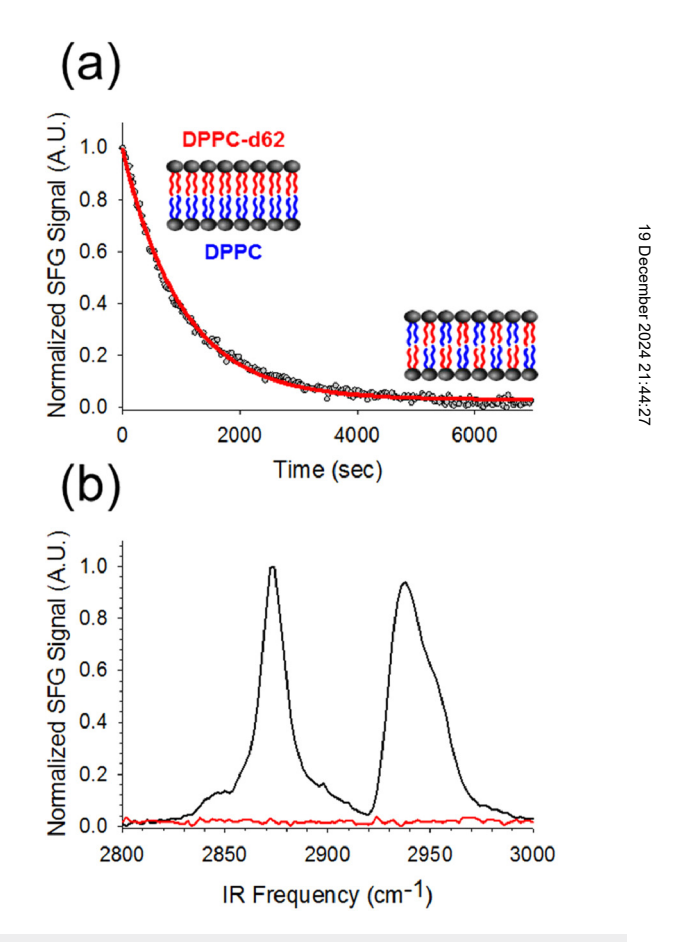


FIG. 7. (a) As proteated and deuterated lipids flip and flop through the membrane, the SFVS signal begins to decay due to the increase in membrane symmetry. (b) SFVS spectra of the asymmetric DPPC/DPPC-d62 membrane before (black) and after (red) complete mixing has occurred.

of the SFVS signal. If the CH₃ v_s mode is probed specifically, the tensor component of $\chi^{(2)}$ associated with the CH₃ v_s mode can be expressed as the sum of the terminal methyl groups found in each leaflet of the PSLB,

$$\chi^{(2)} = \frac{N_{\text{distal}}}{\varepsilon_0} \beta^{CH_3 \nu_s} - \frac{N_{\text{proximal}}}{\varepsilon_0} \beta^{CH_3 \nu_s}, \tag{11}$$

where N_{distal} and N_{proximal} are the number of proteated, SFVS active lipids in the distal and proximal leaflets, respectively, ε_0 is the vacuum permittivity, and $\beta^{CH_3v_s}$ is the hyperpolarizability of the CH₃ v_s transition. The negative sign signifies the opposing orientation (and phase), the CH₃ v_s transition in the proximal and distal leaflets. By convention, the proximal leaflet refers to the leaflet closest to the solid support (the LB layer), while the distal leaflet refers to the leaflet furthest from the solid support (the LS layer). Equation (11) shows that $\chi^{(2)}$ is influenced by the number of proteated lipids in each leaflet, and as the number of proteated lipids in each leaflet approaches equality, $\chi^{(2)}$ approaches zero.

The flip-flop of distal and proximal lipids can be represented

$$N_{\text{distal}} \stackrel{k_{+}}{\rightleftharpoons} N_{\text{proximal}},$$
 (12)

with k_+ and k_- being the forward and reverse flip-flop rate constants, respectively. For asymmetric bilayers, there are initially proteated lipids exclusively in one leaflet ($N_{\rm distal}=1$) and deuterated lipids in the other leaflet ($N_{\text{proximal}} = 0$), and the timedependent change of N_{distal} is given by

$$\frac{dN_{\text{distal}}}{dt} = k_{-}N_{\text{proximal}} - k_{+}N_{\text{distal}}.$$
 (13)

It has been shown that k_- and k_+ are equal for phospholipid flip-flop in PSLBs,²¹ and as a result, Eq. (13) can be reduced to the following:

$$\frac{dN_{\text{distal}}}{dt} = -k(2N_{\text{distal}} - 1). \tag{14}$$

Equation (14) can be rearranged and integrated to give the rate expression for lipid flip-flop,

$$2N_{\text{distal}}(t) - 1 = e^{(-2kt)}. (15)$$

SFVS is proportional to the square of the number of molecules at the surface [Eq. (2)] and Eq. (15) can be merged into Eq. (11) to give

$$I_{CH_3}(t) = I_{\text{max}}e^{-4kt} + I_0,$$
 (16)

where $I_{CH_3}(t)$ is the time-dependent SFVS signal intensity of the terminal methyl group at 2876 cm^{-1} , I_{max} is the maximum SFVS signal intensity, k is the flip-flop rate constant, and I_0 is a signal minimum associated with a fully symmetric bilayer when N_{distal} equals N_{proximal} and is caused by a nonresonant signal and instrument offset. A full derivation of the rate expression can be found elsewhere.²¹ The rate of SFVS signal decay can be modeled using Eq. (16) (see Sec. III) at a particular temperature to determine the rate constant k for flip-flop at that temperature. The rate constant can then be used to determine a half-life for lipid flip-flop using

$$t_{\frac{1}{2}} = \frac{\ln(2)}{2k}. (17)$$

Lastly, the rates determined from SFVS decays can be used to obtain meaningful activation thermodynamics for lipid flip-flop using transition state theory (TST).⁸⁰ An activation barrier to flipflop exists as the movement of the hydrophilic head group through the hydrophobic core of a membrane is not favorable. The activation barrier to flip-flop is represented by an activation free energy (ΔG^{\ddagger}) that has enthalpic and entropic contributions. Using Eyring theory, 80 the rates obtained from SFVS decay experiments can be used to determine ΔG^{\ddagger} ,

$$k = \frac{k_B T}{h} e^{-\frac{\Delta G^{\frac{1}{L}}}{RT}},\tag{18}$$

where k_B is Boltzmann's constant, T is the temperature at which the rate for flip-flop was collected in kelvin, h is Planck's constant, and R is the ideal gas constant. The enthalpic and entropic contributions to the activation barrier can be calculated from the Gibbs equation,

$$\Delta G^{\ddagger} = \Delta H^{\ddagger} - T\Delta S^{\ddagger}. \tag{19}$$

With these concepts and equations in hand, one can determine $\frac{8}{2}$ the rate and activation thermodynamics of flip-flop. Select examples $\stackrel{N}{:}$ of using SFVS for the determination of lipid flip-flop kinetics are found in Sec. IV.

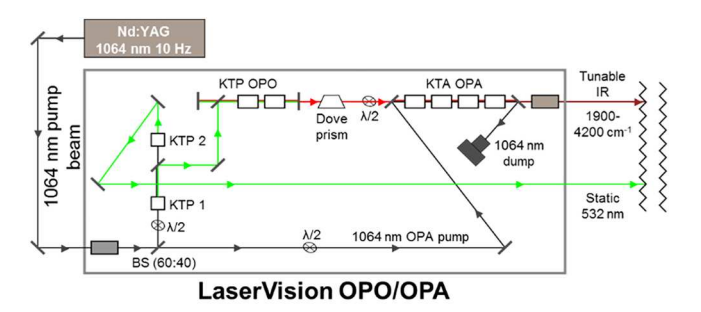
C. Instrumentation

Before discussing the instrumentation and the use of lasers, in particular, it is important to stress laboratory and laser safety. It is crucial for anyone operating a laser system to become very familiar with the risks and dangers that are associated with working with lasers. SFVS uses class IV lasers that are especially dangerous if misused. The authors encourage those interested in working with laser systems to exercise due diligence in familiarizing themselves with the appropriate safety information before constructing or operating a laser system. Only a brief description of the laser system used in our laboratory will be provided here in order to give a sense of the instrumentation needed to make these types of measurements, and the information provided is by no means an exhaustive description. Obviously, different laboratories have varying types of equipment, and the instrumentation described here is not intended to be a requirement nor an endorsement of any particular type of instrumentation or manufacturer. The instrumentation will be broken down into two parts: first, the laser system used to generate the incoming visible and IR laser beams,

and second, the data acquisition instrumentation that converts the SFVS signal into interpretable data.

1. Laser system

The laser system used in our laboratory is a custom-made spectrometer consisting of a fixed frequency visible source at 532 nm and a tunable IR source generated by an optical parametric oscillator (OPO)/optical parametric amplifier (OPA) from LaserVision (Bellevue, WA). The OPO/OPA system is pumped with a Q-switched Nd:YAG laser such as a Continuum Surelite III (Amplitude, Santa Clara, CA) or a Spectra-Physics Quantaray Pro (MKS Instruments, Andover, MA) that has a 1064 nm output at a repetition of 10 Hz with a pulse duration of 7 ns and an energy of ~450 mJ/pulse. The 1064 nm source is frequencydoubled through a KTP crystal to generate a 532 nm pump source for the OPO/OPA, which generates a tunable mid-IR with a frequency range of 2000-4200 cm⁻¹. Residual 1064 nm is also frequency-doubled to produce our 532 nm visible source that is used for SFVS, which can be seen in Fig. 8. The power intensities for the IR and 532 nm at the surface are set to approximately 4 and 6 mJ/pulse, respectively. The tunable IR and 532 nm beams are collimated to a beam diameter of ~4 and ~3 mm, respectively, and aligned to both spatially and temporally overlap at the silica surface under TIR at 69° and 63° for the IR and 532 nm, respectively. To easily visualize the IR source when aligning the instrument, a HeNe laser is aligned to the IR source. Several filters are used to remove the reflected IR and 532 nm so that only the reflected sum-frequency photons can reach a photomultiplier tube (PMT) (Hamamatsu Photonics, Shizuoka, Japan) for



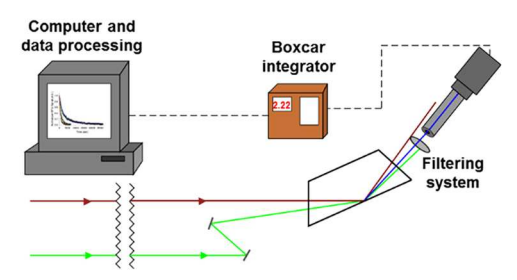


FIG. 8. Illustrative schematic of the laser system and data processing. Some optics have been removed for clarity. The angles in this figure are not accurate and are for illustrative purposes only.

detection. These filters include bandpass filters (Thorlabs, NJ) that transmit the sum-frequency range (457-464 nm) and 532 nm notch filters (Semrock, Rochester, NY) to eliminate any residual 532 nm, as this is the primary source of noise that reaches the PMT. To eliminate noise further, a spatial filter can be placed before the PMT.

The use of a nanosecond pulsed Nd:YAG source with a LaserVision system produces a tunable IR beam with a narrow bandwidth of ~2 cm -1 and requires tuning of the OPO/OPA at each individual IR frequency. A more commonly encountered laser system used to collect SFVS spectra are femtosecond pulsed Ti: Sapphire lasers, which have the benefit of being broadband. 66,81-Both systems have their benefits and drawbacks. In terms of collecting spectra, the nanosecond system needs to scan each individual frequency and integrate over that frequency, while the femtosecond system collects pieces of the spectra all at once. Depending on the femtosecond system, tuning of the broadband frequency to collect the entire spectral region of interest may require integrating over two or sometimes three frequency ranges, which slows down the process. Depending on the length of the integration time, the time required to collect a spectrum is comparable between the two systems. However, as mentioned previously, flip-flop begins to occur at the conception of the PSLB, which can influence the collection of SFVS spectra if the rate of flip-flop is rapid. The time needed to collect the spectrum needs to be highly considered and an appropriate temperature of the bilayer chosen such that the an appropriate temperature bilayer does not undergo an appreciable amount or imperior the course of the collection of the spectrum. Another aspect of the two systems is the detection system used. The nanosecond system of the spectrum while the femtosecond systems of the amplification of the spectrum. use a charge-coupled device (CCD) that does not have the amplification that PMTs possess. However, the nanosecond systems have a second systems have a repetition rate only at 10 Hz, while that of the femtosecond systems is on the order of kilohertz, balancing out the integration times $\frac{2}{N}$ required. Ultimately, the systems are comparable, and which system one wishes to use will depend on preference and application.

2. Data acquisition system

The SFVS signal reaches a PMT and this signal is amplified and collected with a boxcar integrator (Stanford Research Systems, Sunnyvale, CA) that is recorded and processed by a data acquisition (DAQ) system (National Instruments, Austin, TX) using LabVIEW. A boxcar integrator is used to measure the SFVS photons within the fixed gate of the integrator (typically 20 ns) and applies a boxcar average to the data improving signal to noise. The typical process of data acquisition for the collection of SFVS spectra is carried out by scanning over the aliphatic carbon-hydrogen vibrational mode region ranging from 2750 to 3050 cm⁻¹ at 2 cm⁻¹ increments averaging 10 s (100 laser pulses) per increment. Typical flip-flop kinetic experiments are conducted by measuring the decay in the SFVS signal at the CH₃ v_s mode at 2876 cm⁻¹, as well as the temperature at the surface, using a thermocouple as a function of time. Both signal intensity and temperature are averaged over 30 s intervals. The raw data collected in LabVIEW are then exported and additional data processing is conducted if necessary.

III. DATA ANALYSIS

Data analysis and fitting of the SFVS spectra and SFVS decays are necessary to determine phospholipid orientation and flip-flop kinetics, respectively. The analysis of SFVS decays uses simple regression analysis, while the fitting of spectra requires the use of peak fitting to Eq. (4). Other types of modeling are required from time to time, but these will not be discussed here. One is encouraged to always become familiar with the data analysis routines needed for any experiment one wishes to collect.

A. Fitting SFVS spectra

SFVS spectra collected in the aliphatic region (2750-3050 cm⁻¹) have multiple sum-frequency active modes that overlap with one another to varying degrees. As such, modeling the individual peaks allows one to obtain the amplitude of a particular vibrational mode, which is critical for determining important values such as $\chi^{(2)}$ for tilt angle measurements. To fit the SFVS spectra, one must have a knowledge of the contributing modes within the spectra. These peaks in the aliphatic region are discussed in detail within the Results section and can be seen in Fig. 9. Once data are collected, each of the five individual peaks in the spectrum is fit to Eq. (4), solving for ω_{IR} , Γ_x , and the peak amplitude, which correspond to the transition probabilities, AkMiix. An examination of Eq. (4) shows that the peak fitting program used must be capable of fitting values with complex numbers, which can be accomplished in programs such as MatLab, Python, or Octave. Fitting SFVS spectra is a nontrivial exercise, as the nonlinear nature of the spectra introduces complexity such as intricate interference effects between adjacent vibrational modes. Additional reading is provided for those interested in a more thorough examination on modeling different types of SFVS spectra.

B. Fitting flip-flop SFVS decays

SFVS decay due to flip-flop in an asymmetric bilayer can be described by way of Eq. (16). The raw data can be fit to Eq. (16) using a nonlinear least squares regression that is available in a variety of programs such as Microsoft Excel, LabPlot, SigmaPlot, Octave, Python, or MatLab. The fitting of the exponential SFVS decay data is a straightforward process and can readily be automated once one understands the theory surrounding the SFVS decay as well as the variables that contribute to the fitting process.

IV. RESULTS AND DISCUSSION

A. Phospholipid orientation experiments

The tilt angle of the terminal methyl groups and choline headgroups of 1,2-distearoyl-sn-glycero-3-phosphocholine (DSPC) were obtained by analyzing the SFVS spectra of PSLBs. The following data are from Liu and Conboy, and the figures and tables given have been modified and reproduced with permission.⁴⁴ Figure 9 shows spectra of a DSPC-d13/DSPC-d83 bilayer obtained using ssp [Fig. 9(a)] and sps [Fig. 9(b)]. The ssp and sps polarization combinations probe the vibrational modes parallel and perpendicular to the membrane surface normal, respectively. All spectra were collected at room temperature where the change in signal due to flip-flop is insignificant for DSPC ($t_{1/2} = 10$ weeks). Fitting the spectra using Eq. (4), we can obtain the amplitudes and peak widths for each individual vibrational mode contributing to the SFVS spectrum. The peak assignments for the ssp spectrum are the following. The peaks seen at 2848 and 2876 cm⁻¹ are the methylene symmetric stretch (CH₂ v_s) and methyl symmetric stretch (CH₃ v_s), respectively. A small shoulder peak at approximately 2905 cm⁻¹ is attributed to the CH₂ fermi (CH₂ FR) resonance and a peak at 2950 cm⁻¹ is a second to the CH₂ fermi (CH₂ FR) at 2938 cm⁻¹ 8 combination of the CH₃ Fermi resonance (CH₃ FR) at 2938 cm⁻¹ and the CH₃ antisymmetric stretch (CH₃ v_{as}) at 2960 cm⁻¹.



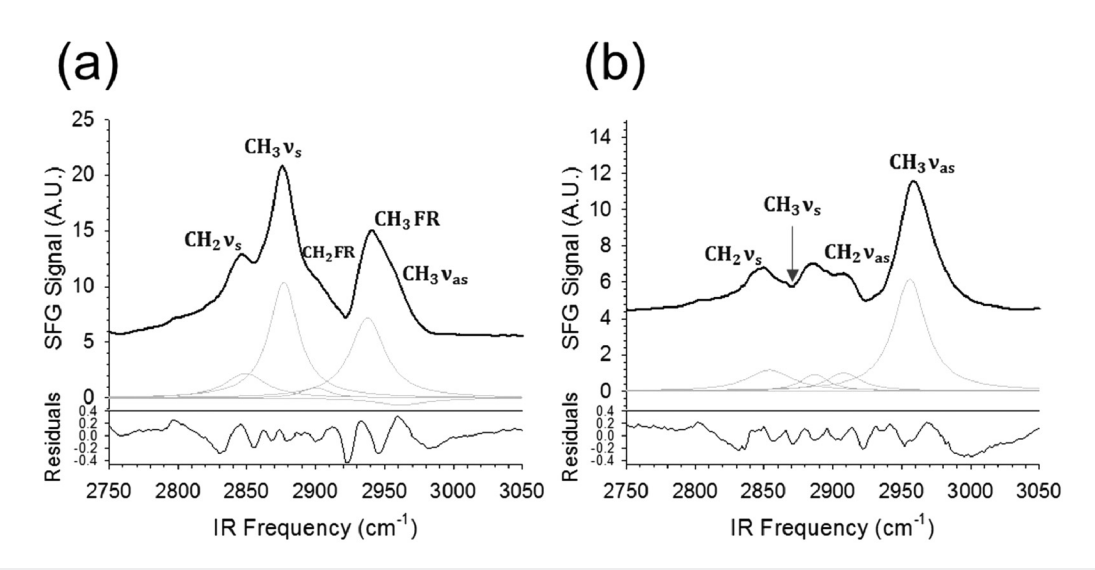


FIG. 9. (a) SFVS spectrum of a DSPC-d13/DSPC-d83 PSLB using ssp polarization and (b) an SFVS spectrum of a DSPC-d13/DSPC-d83 PSLB using sps polarization. Adapted with permission from Liu and Conboy, Langmuir 21, 9091 (2005) (Ref. 44). Copyright 2005, American Chemical Society.

These peak assignments have been corroborated by our group as ⁻⁸⁸ The *sps* spectrum peak assignments are the well as others.^{21,8} following: the weak resonances at 2850, 2890, and 2912 cm⁻¹ are the CH₂ v_s, the C-H resonance from the chiral center of the glycerol group, and the CH2 vas mode, respectively, and the predominant peak at 2960 cm $^{-1}$ is the CH $_3$ v $_{as}$ mode. He To determine the terminal CH $_3$ tilt angle, the peak at 2876 cm $^{-1}$ (CH $_3$ v $_s$ mode) was included in the fitting of the sps spectrum to determine the relative SFVS amplitude in that region. The amplitudes of the fits at 2876 cm⁻¹ for the ssp and sps spectra were 41.15 and 0.125, respectively.

With the amplitudes from the fits and Fresnel coefficients calculated using our knowledge of the incident angles and the refractive indices of our system, we can determine $\chi^{(2)}_{ssp}$ and $\chi^{(2)}_{sps}$ using Eqs. (9) and (10), respectively. The ratio between $\chi^{(2)}_{ssp}$ and $\chi_{sps}^{(2)}$ can then be used in Eq. (7) to determine the tilt angle of the terminal CH₃ group on the alkyl chains of the PSLB. The following amplitudes and incident angles determined from these spectra give a CH₃ tilt angle of 22.7° with respect to the surface normal. Using simple geometry, the CH3 tilt can be used to determine the tilt angle of the alkyl chains of the phospholipids of the bilayer, which gives a chain tilt angle of 12° assuming an all-trans configuration of the lipid tails, which is in excellent agreement with both molecular dynamic simulations and experimental studies using neutron reflectometry and x-ray diffraction.⁸⁹⁻⁹⁴ Similar spectra can be obtained to determine the tilt angle of the choline head group (data not given), which was shown to be 69° ± 3° using SFVS, which is also in agreement with previously reported values between 50° and When looking at the alkyl chain and choline headgroup tilt angles in the proximal and distal leaflets, it was found that the tilt angles are within error of each other.44 This suggests that the deposition order does not drastically influence the molecular ordering of the bilayer nor does the charged silica substrate have a substantial influence on proximal leaflet orientation. These results are in support of the growing evidence that PSLBs make good in vitro models for lipid bilayers.

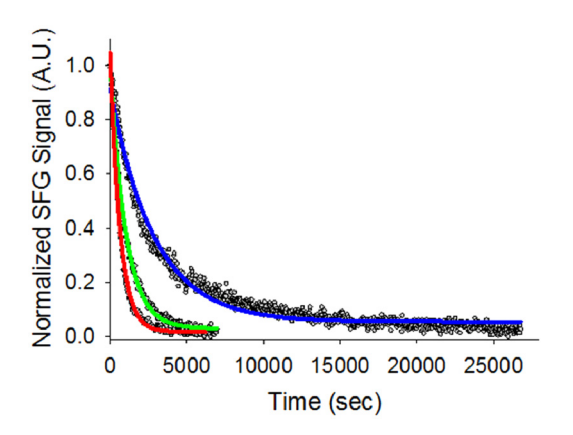


FIG. 10. Example SFVS decays of an asymmetric DPPC/DPPC-d62 PSLB at 28.3°C (blue), 33.1°C (green), and 35.3°C (red). The lines are exponential fits to the raw data using Eq. (16).

TABLE I. Rate of flip-flop and corresponding half-lives for DMPC, DPPC, and DSPC. Adapted with permission from Liu and Conboy, Biophys. J. 89, 2522 (2005) (Ref. 21). Copyright 2005, Cell Press.

	Temperature (°C)	Rate $(k \times 10^5)$	t _{1/2} (min)
DMPC	4.2 ± 0.4	2.56 ± 0.06	226 ± 5
	7.8 ± 0.1	7.04 ± 0.05	82.0 ± 0.6
	9.8 ± 0.1	16.7 ± 0.17	34.6 ± 0.4
	12.1 ± 0.1	68.6 ± 0.87	8.42 ± 0.11
	15.8 ± 0.2	196 ± 5.82	2.95 ± 0.09
	20.4 ± 0.3	443 ± 10.1	1.30 ± 0.03
DPPC	27.7 ± 0.1	3.95 ± 0.02	146 ± 1
	29.7 ± 0.1	8.04 ± 0.02	71.8 ± 0.2
	30.5 ± 0.1	11.6 ± 0.03	49.8 ± 0.1
	31.5 ± 0.1	15.5 ± 0.05	37.3 ± 0.1
	32.3 ± 0.1	18.9 ± 0.07	30.5 ± 0.1
	36.0 ± 0.1	42.2 ± 0.29	13.7 ± 0.1
	36.6 ± 0.1	62.8 ± 0.51	9.20 ± 0.07
DSPC	41.7 ± 0.3	1.85 ± 0.01	312 ± 2
	44.5 ± 0.3	3.60 ± 0.01	160 ± 1
	45.7 ± 0.3	4.67 ± 0.02	142 ± 1
	46.3 ± 0.4	6.72 ± 0.01	86.0 ± 0.1
	49.2 ± 0.2	8.35 ± 0.02	69.2 ± 0.2
	50.3 ± 0.1	15.2 ± 0.06	38.1 ± 0.2
	51.3 ± 0.2	22.3 ± 0.07	25.9 ± 0.1

B. Phospholipid flip-flop experiments

An analysis of phospholipid flip-flop through SFVS decays was conducted on 1,2-dimyristoyl-sn-glycero-3-phosphocholine (DMPC), DPPC, and DSPC and the corresponding activation thermodynamics were related. modynamics were calculated. An example of SFVS decay as a result of lipid flip-flop can be seen in Fig. 10, where the decays of a DPPC/DPPC-d62 PSLB at three different temperatures were measured. Table I shows the temperature, flip-flop rate, and

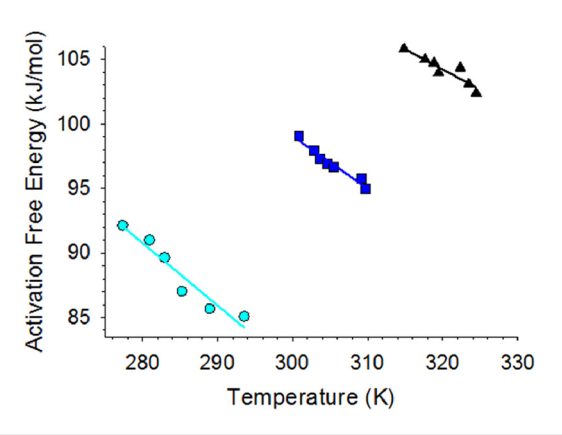


FIG. 11. Gibbs plots for a series of asymmetric PSLB flip-flop experiments of DMPC (cyan circles), DPPC (blue squares), and DSPC (black triangles). These Gibbs plots were generated from rates found in Liu and Conboy (Ref. 21).

TABLE II. Gibbs activation energy, activation enthalpy, and activation entropy for DMPC, DPPC, and DSPC at 20.9 °C. Adapted with permission from Anglin *et al.*, J. Phys. Chem. B 114, 1903 (2010) (Ref. 42). Copyright 2010, American Chemical

	ΔG^{\ddagger} (kJ/mol)	ΔH^{\ddagger} (kJ/mol)	ΔS [‡] (J/mol K)
DMPC	84 ± 1	251 ± 14	167 ± 12
DPPC	100.7 ± 0.3	245 ± 10	143 ± 8
DSPC	113 ± 4	243 ± 29	130 ± 28

corresponding half-lives of DMPC, DPPC, and DSPC, which are lipids containing 14, 16, and 18 carbon alkyl chains, respectively, with a choline headgroup. It can be seen that there is a noticeable temperature dependence on the flip-flop rates for the different chain lengths. In all three, the gel phase half-lives are on the order of hours to minutes, and as we approach the phase transition into the liquidcrystalline phase, the half-lives are on the order of a few minutes. It should be noted that flip-flop measurements above the phase transition are not possible using SFVS, as a complete mixing of the proteated and deuterated lipids occurs too quickly to measure (<1 min). These results suggest that flip-flop is a fast process, even in the gel phase, and most likely occurs rapidly in the liquid-crystalline phase. This would indicate that native flip-flop is a fast process and could have significant biological importance.

Activation thermodynamics such as the activation barrier to flip-flop can be calculated using the rates of flip-flop in conjunction with Eyring theory [Eq. (18)]. Figure 11 shows the Gibbs plot that is made using Eq. (18). The Gibbs equation [Eq. (19)] is then used to determine the activation enthalpy and entropy for DMPC, DPPC, and DSPC at a particular temperature. The activation thermodynamics for DMPC, DPPC, and DSPC are presented in Table II, and there is a clear relationship between the activation thermodynamics and chain length with an increase in ΔG^{\ddagger} from 84, 100.7, to 113 for DMPC, DPPC, and DSPC, respectively. There is an approximately 13 kJ/mol increase in the activation free energy of flip-flop per two carbon addition to the aliphatic chain. The change in the free energy of activation is due in large part to a decrease in the ΔS^{\dagger} with the increase in chain length, while there is no statistical difference in the ΔH^{\ddagger} .

V. SUMMARY AND CONCLUSIONS

Sum-frequency is a powerful tool for the measurement of membrane structures and kinetics due to the unique symmetry requirements for SFVS. Through the use of PSLBs, an asymmetric distribution of isotopically labeled lipids makes SFVS possible on bilayers and allows for the measurement of a variety of membrane characteristics such as chain and headgroup orientation as well as kinetic phenomena such as phospholipid flip-flop. The examples given in this tutorial are a brief introduction to what can be done using SFVS and PSLBs, and many other applications exist. Through the use of sum-frequency, the rates of flip-flop of a variety of native lipids can be measured and compared with labeled lipids to draw a conclusion on the efficacy of these labeled lipids.²¹ Likewise, other factors that can influence flip-flop, such as phospholipid headgroup, lateral surface pressure and membrane packing;

chemical reagents, and other relevant membrane constituents such as cholesterol, fatty acids, and vitamin E, can be included in the PSLB to determine the influence that these factors have on kinetics and thermodynamics. 37-41,47,48 Other important measurements such as the desorption and adsorption of a variety of biomolecules from and to the membrane surface can be measured using the incredible surface sensitivity of SFVS. 39,49 Sum-frequency has many unique aspects that make it a strong analytical tool to measure a variety of surface-related questions, including those surrounding the behavior of membranes. It is hoped that this brief Tutorial on the use of sum-frequency to measure membrane kinetics stimulates creativity or inspiration to those who wish to enter the world of NLO to make such measurements.

ACKNOWLEDGMENTS

This work was supported by the National Science Foundation (NSF) (No. 1953975).

AUTHOR DECLARATIONS

Conflict of Interest

The authors have no conflicts to disclose.

Ethics Approval

Ethics approval is not required.

Author Contributions

Joshua M. Taylor: Conceptualization (equal); Data curation (equal); Formal analysis (equal); Investigation (equal); Methodology (equal); Validation (equal); Writing – original draft (equal). **John C. Conboy:** Conceptualization (equal); Data curation (equal); Formal analysis (equal); Funding acquisition (equal); $\frac{1}{4}$ Investigation (equal); Methodology (equal); Project administration (equal); Resources (equal); Supervision (equal); Validation (equal); Writing - review & editing (equal).

DATA AVAILABILITY

The data that support the findings of this study are available from the corresponding author upon reasonable request.

REFERENCES

¹Robert Hooke, Micrographia: Or Some Physiological Description of Minute Bodies Made by Magnifying Glasses with Observations and Inquiries Thereupon (Martyn and J. Allestry, The Royal Society, London, 1665).

²L. J. Gibson, K. E. Easterling, and M. F. Ashby, Proc. R. Soc. A 377, 99 (1981).

³A. van Leeuwenhoek, Philos. Trans. R. Soc. 12, 821 (1677).

⁴N. Lane, Philos. Trans. R. Soc. B Biol. Sci. **370**, 20140344 (2015).

⁵J. Lombard, Biol. Direct 9, 1 (2014).

⁶H. M. Keşfi, Bezmialem Sci. **8**, 81 (2020).

⁷S. J. Singer and G. L. Nicolson, Science 175, 720 (1972).

⁸D. M. Engelman, Nature **438**, 578 (2005).

⁹A. H. Maddy, Biochim. Biophys. Acta Biomembr. 88, 390 (1964).

¹⁰P. F. Devaux, Biochemistry **30**, 1163 (1991).

¹¹G. Van Meer, D. R. Voelker, and G. W. Feigenson, Nat. Rev. Mol. Cell Biol. 9, 112 (2008).

¹²A. Yamaji-Hasegawa and M. Tsujimoto, Biol. Pharm. Bull. **29**, 1547 (2006).

⁵⁸P. S. Cremer and S. G. Boxer, J. Phys. Chem. B **103**, 2554 (1999).
 ⁵⁹E. T. Castellana and P. S. Cremer, Surf. Sci. Rep. **61**, 429 (2006).
 ⁶⁰J. C. Conboy, S. Liu, D. F. O'Brien, and S. S. Saavedra, Biomacromolecules **4**, 841 (2003).

57H. M. McConnell, T. H. Watts, R. M. Weis, and A. A. Brian, Biochim.

- ⁶¹J. M. Smaby, V. S. Kulkarni, M. Momsen, and R. E. Brown, Biophys. J. **70**, 868 (1996).
- 62 Y. R. Shen, The Principles of Nonlinear Optics (Wiley, New York, 1985).
- 63 R. Boyd, Nonlinear Optics, 3rd ed. (Academic Press, Cambridge, 2008).
- 64A. G. Lambert, P. B. Davies, and D. J. Neivandt, Appl. Spectrosc. Rev. 40, 103 (2005)
- 65J. D. Pickering, M. Bregnhøj, A. S. Chatterley, M. H. Rasmussen, K. Strunge, and T. Weidner, Biointerphases 17, 011201 (2022).
- ⁶⁶J. D. Pickering, M. Bregnhøj, A. S. Chatterley, M. H. Rasmussen, S. J. Roeters, K. Strunge, and T. Weidner, Biointerphases 17, 011202 (2022).
- 67 J. D. Pickering, M. Bregnhøj, M. H. Rasmussen, K. Strunge, and T. Weidner, Biointerphases 17, 041201 (2022).
- ⁶⁸B. Dick, A. Gierulski, G. Marowsky, and G. A. Reider, Appl. Phys. B Photophys. Laser Chem. **38**, 107 (1985).
- 69 M. J. Hofmann and P. Koelsch, J. Chem. Phys. 143, 134112 (2015).
- ⁷⁰I. H. Malitson, J. Opt. Soc. Am. 55, 1205 (1965).

Biophys. Acta Rev. Biomembr. 864, 95 (1986).

- ⁷¹ J. J. Max and C. Chapados, J. Chem. Phys. 131, 184505 (2009).
- 72S. Kedenburg, M. Vieweg, T. Gissibl, and H. Giessen, Opt. Mater. Express 2, 1588 (2012).
- ⁷³J. Martín and S. Montero, J. Chem. Phys. **80**, 4610 (1984).
- 74D. Zhang, J. Gutow, and K. B. Eisenthal, J. Phys. Chem. 98, 13729 (1994).
- 75 H. I. Petrache, S. W. Dodd, and M. F. Brown, Biophys. J. 79, 3172 (2000).
- ⁷⁶A. Salmon, S. W. Dodd, G. D. Williams, J. M. Beach, and M. F. Brown, J. Am. Chem. Soc. **109**, 2600 (1987).
- ⁷⁷J. Liu and J. C. Conboy, J. Phys. Chem. C 111, 8988 (2007).
- ⁷⁸J. H. Davis, <u>BBA Rev. Biomembr.</u> 737, 117 (1983).
- ⁷⁹J. Seelig and A. Seelig, Q. Rev. Biophys. **13**, 19 (1980).
- 80H. Eyring, Chem. Rev. 17, 65 (1935).
- 81 L. J. Richter, T. P. Petralli-Mallow, and J. C. Stephenson, Opt. Lett. 23, 1594 (1998).
- 82 E. L. Hommel and H. C. Allen, Anal. Sci. 17, 137 (2001).
- 83 D. Bodlaki and E. Borguet, Rev. Sci. Instrum. 71, 4050 (2000).
- 84 L. Yang, W. Zhang, H. Bian, and G. Ma, Biointerphases 17, 051201 (2022).
- ⁸⁵M. G. Brown, E. A. Raymond, H. C. Allen, L. F. Scatena, and G. L. Richmond, J. Phys. Chem. A **104**, 10220 (2000).
- ⁸⁶A. D. Quast, N. C. Wilde, S. S. Matthews, S. T. Maughan, S. L. Castle, and J. E. Patterson, Vib. Spectrosc. **61**, 17 (2012).
- 87 M. C. Henry, L. K. Wolf, and M. C. Messmer, J. Phys. Chem. B 107, 2765 (2003).
- 88 R. A. Walker, J. C. Conboy, and G. L. Richmond, Langmuir 13, 3070 (1997).
- 89 C. Bolterauer and H. Heller, Eur. Biophys. J. 24, 322 (1996).
- 90 I. Burgess, M. Li, S. L. Horswell, G. Szymanski, J. Lipkowski, S. Satija, and J. Majewski, Colloids Surf. B Biointerfaces 40, 117 (2005).
- ⁹¹ A. Tardieu, V. Luzzati, and F. C. Reman, J. Mol. Biol. 75, 711 (1973).
- 92M. J. Janiak, D. M. Small, and G. G. Shipley, J. Biol. Chem. 254, 6068 (1979).
- 93T. J. McIntosh and S. A. Simon, Biochemistry 32, 8374 (1993).
- 94 R. H. Pearson and I. Pascher, Nature 281, 499 (1979).
- 95W. Hübner and H. H. Mantsch, Biophys. J. 59, 1261 (1991).
- 96H. Binder, T. Gutberlet, A. Anikin, and C. V. Klose, Biophys. J. 74, 1908 (1998).
- 97 P. L. Yeagle, Acc. Chem. Res. 11, 321 (1978).
- 98H. Akutsu, M. Ikematsu, and Y. Kyogoku, Chem. Phys. Lipids 28, 149 (1981).
- ⁹⁹E. Okamura, J. Umemura, and T. Takenaka, Biochem. Biophys. Acta 1025, 94 (1990).
- 100 L. Ter-Minassian-Saraga, E. Okamura, J. Umemura, and T. Takenaka, Biochem. Biophys. Acta 946, 417 (1988).
- ¹⁰¹G. Buldt, H. U. Galley, J. Seelig, and G. Zaccai, J. Mol. Biol. 134, 673 (1979).
- ¹⁰²J. S. Allhusen and J. C. Conboy, Acc. Chem. Res. **50**, 58 (2017).

- ¹³M. Ikeda, A. Kihara, and Y. Igarashi, Biol. Pharm. Bull. **29**, 1542 (2006).
- 14J. A. F. Op den Kamp, Annu. Rev. Biochem. 48, 47 (1979).
- ¹⁵C. F. Higgins, Cell **79**, 393 (1994).
- ¹⁶R. J. Clarke, K. R. Hossain, and K. Cao, Biochim. Biophys. Acta Biomembr. 1862, 183382 (2020).
- ¹⁷P. F. Devaux and A. Herrmann, *Transmembrane Dynamics of Lipids* (Wiley, New York, 2011).
- ¹⁸X. Tang, M. S. Halleck, R. A. Schlegel, and P. Williamson, Science 272, 1495 (1996)
- ¹⁹T. Pomorski, R. Lombardi, H. Riezman, P. F. Devaux, G. Van Meer, and J. C. M. Holthuis, Mol. Biol. Cell 14, 1240 (2003).
- ²⁰C. Y. Chen, M. F. Ingram, P. H. Rosal, and T. R. Graham, J. Cell Biol. **147**, 1223 (1999).
- ²¹ J. Liu and J. C. Conboy, Biophys. J. **89**, 2522 (2005).
- ²²J. Bai and R. E. Pagano, Biochemistry **36**, 8840 (1997).
- ²³R. D. Kornberg and H. M. McConnell, Biochemistry **10**, 1111 (1971).
- ²⁴P. F. Devaux, P. Fellmann, and P. Hervé, Chem. Phys. Lipids **116**, 115 (2002).
- ²⁵D. W. C. Dekkers, P. Comfurius, A. J. Schroit, E. M. Bevers, and R. F. A. Zwaal, Biochemistry 37, 14833 (1998).
- ²⁶S. Hrafnsdóttir, J. W. Nichols, and A. K. Menon, Biochemistry 36, 4969 (1997)
- 27T. Pomorski, P. Müller, B. Zimmermann, K. Burger, P. F. Devaux, and A. Herrmann, J. Cell Sci. 109, 687 (1996).
- ²⁸R. Homan and H. J. Pownall, Biochim. Biophys. Acta Biomembr. 938, 155 (1988).
- 29M. Nakano, M. Fukuda, T. Kudo, N. Matsuzaki, T. Azuma, K. Sekine, H. Endo, and T. Handa, J. Phys. Chem. B 113, 6745 (2009).
- ³⁰M. Nakano, M. Fukuda, T. Kudo, H. Endo, and T. Handa, Phys. Rev. Lett. 98, 238101 (2007).
- ³¹D. Marquardt, F. A. Heberle, T. Miti, B. Eicher, E. London, J. Katsaras, and G. Pabst, Langmuir 33, 3731 (2017).
- 32J. Liu and J. C. Conboy, J. Am. Chem. Soc. 126, 8376 (2004).
- 33 L. K. Tamm and H. M. McConnell, Biophys. J. 47, 105 (1985).
- ³⁴A. L. Plant, Langmuir **15**, 5128 (1999).
- 35M. L. Wagner and L. K. Tamm, Biophys. J. 79, 1400 (2000).
- **36**T. V. Ratto and M. L. Longo, Biophys. J. **83**, 3380 (2002).
- ³⁷J. Liu, K. L. Brown, and J. C. Conboy, Faraday Discuss. **161**, 45 (2013).
- 38 K. L. Brown and J. C. Conboy, J. Phys. Chem. B 117, 15041 (2013).
- ³⁹V. Cheng, D. R. Kimball, and J. C. Conboy, J. Phys. Chem. B 123, 7157 (2019).
- ⁴⁰V. Cheng, R. Rallabandi, A. Gorusupudi, S. Lucas, G. Rognon, P. S. Bernstein, J. D. Rainier, and J. C. Conboy, Biophys. J. 121, 2730 (2022).
- ⁴¹V. Cheng and J. C. Conboy, J. Phys. Chem. B **126**, 7651 (2022).
- ⁴²T. C. Anglin, M. P. Cooper, H. Li, K. Chandler, and J. C. Conboy, J. Phys. Chem. B 114, 1903 (2010).
- ⁴³J. Liu and J. C. Conboy, J. Am. Chem. Soc. **126**, 8894 (2004).
- ⁴⁴J. Liu and J. C. Conboy, Langmuir **21**, 9091 (2005).
- ⁴⁵J. Liu and J. C. Conboy, J. Phys. Chem. B **119**, 10252 (2015).
- ⁴⁶T. C. Anglin, J. Liu, and J. C. Conboy, Biophys. J. **92**, L01 (2007).
- ⁴⁷T. C. Anglin and J. C. Conboy, Biophys. J. **95**, 186 (2008).
- 48 T. C. Anglin and J. C. Conboy, Biochemistry 48, 10220 (2009).
- 49T. T. Nguyen, K. Rembert, and J. C. Conboy, J. Am. Chem. Soc. 131, 1401 (2009)
- 50 K. L. Brown and J. C. Conboy, J. Am. Chem. Soc. 133, 8794 (2011).
- ⁵¹J. Liu and J. C. Conboy, Vib. Spectrosc. **50**, 106 (2009).
- ⁵²J. S. Allhusen, D. R. Kimball, and J. C. Conboy, J. Phys. Chem. B **120**, 3157 (2016)
- 53T. C. Anglin, K. L. Brown, and J. C. Conboy, J. Struct. Biol. 168, 37 (2009).
- 54K. B. Blodgett, J. Am. Chem. Soc. 57, 1007 (1935).
- 55K. B. Blodgett, J. Am. Chem. Soc. 56, 495 (1934).
- ⁵⁶O. N. Oliveira, L. Caseli, and K. Ariga, Chem. Rev. **122**, 6459 (2022).

19 December 2024